LANGMUIR

Article

pubs.acs.org/Langmuir

Anionic Lipid Content Presents a Barrier to the Activity of ROMP-Based Synthetic Mimics of Protein Transduction Domains (PTDMs)

Michael Lis,[†] Franziska Dorner,[§] Gregory N. Tew,*[,†,‡] and Karen Lienkamp*[,§]

[†]Department of Polymer Science and Engineering and [‡]Department of Veterinary and Animal Science, Molecular and Cellular Biology Program, University of Massachusetts Amherst, Amherst, Massachusetts 01003, United States

[§]Department of Microsystems Engineering (IMTEK) and Freiburg Centre for Interactive Materials and Bioinspired Technologies (FIT), Albert-Ludwigs-Universität, Georges-Köhler-Allee 103, 79110 Freiburg, Germany

Supporting Information

ABSTRACT: Many biophysical studies of protein transduction domains (PTDs) and their synthetic mimics (PTDMs) focus on the interaction between the polycationic PTD(M) and anionic phospholipid surfaces. Most, but not all, of these studies suggest that these cation−anion interactions are vital for membrane activity. In this study, the effect of anionic lipid content on PTDM performance was examined for three ring-opening metathesis (ROMP)-based PTDMs with varying hydrophobicity. Using a series of dye-loaded vesicles with gradually increasing anionic lipid content, we saw that increased anionic lipid content inhibited dye release caused by these PTDMs. This result is the opposite of what was found in studies with poly- and oligo-arginine. While the effect is reduced for more hydrophobic PTDMs, it is observable even with the most hydrophobic PTDMs of our test panel. Additional experiments included dynamic light scattering and zeta potential measurements to measure size as a function of vesicle surface charge in the presence of increasing PTDM concentration and surface plasmon resonance spectroscopy to quantify binding between PTDMs and surface-bound lipid layers with varying anion content. The results from these measurements suggested that PTDM hydrophobicity, not cation−anion interactions, is the main driving force of the interaction between our PTDMs and the model membranes investigated. This suggests a model of interaction where surface association and membrane insertion are driven by PTDM hydrophobicity, while anionic lipid content serves primarily to "pin" the PTDM to the membrane surface and limit insertion.

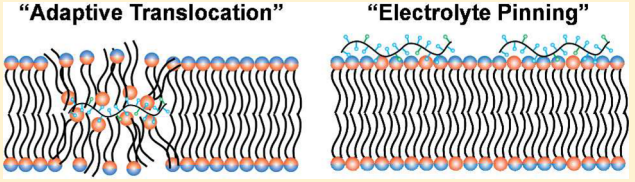

INTRODUCTION

Cells can take up proteins and similar cargo using protein transduction domains (PTDs).[1−7] These peptide segments are parts of cell-penetrating peptides (CPPs) and are generally arginine rich and capable of facilitating transport of large molecules across phospholipid membranes. As summarized by Kim et al., naturally derived CPPs are currently categorized into five classes: cationic CPPs from heparin-, RNA-, and DNA-binding proteins; hydrophobic or amphiphilic CPPs from signal peptides; CPPs derived from antimicrobial peptides; CPPs derived from proteins of microorganisms; and CPPs derived from phages and plasmids display screenings.[8] The field of synthetic mimics of PTDs, i.e., of macromolecules that interact with cell membranes, has been recently reviewed by Marie et al.[9]

The question of how PTDs and their synthetic mimics (PTDMs) shuttle their cargo into cells is a widely debated and still largely controversial topic. The energy-independent mechanisms by which polymers can enter cells are a matter of intense study,[10−15] and there is compelling evidence that at least some polymers are able to cross the lipid bilayer. This happens either when they permeate from outside the cells to the cell's interior or when these polymers escape from endosomes. It was also demonstrated that it is possible to deliver functional biomolecules into the interior of a cell using polymers.[6,7,16] For example, siRNA knockdown of the Notch homologue 1 (NOTCH1) protein through the delivery of sequence-specific siRNA into cells has been demonstrated.[17] More recent work has also shown delivery of fully functional Cre recombinase enzyme into primary human T cells for the knockout of a green fluorescent protein reporter gene located between two DNA recognition (loxP) sites.[18] Studies by other research groups have also demonstrated the delivery of functional biomolecules by covalently bound PTDs.[19−22] Recently, Kim et al. reported a charge-neutral cell-penetrating peptide that was strongly hydrophobic and was more efficiently taken up by cells than the well-known cell-penetrating peptide TAT.[8]

Further biophysical and simulation studies demonstrated the ability of some polymers to cross lipid bilayers without the need for endocytosis.[23−31] Among those biophysical studies, there is strong consensus supporting the importance of the interactions between the cationic polymer and the anionic surface of the cell. Matile and co-workers have demonstrated that oligo- and polyarginine had a dramatically increased membrane activity when they were complexed with amphiphilic anions.[13,23−25]

Received: January 21, 2016
Revised: May 11, 2016
Published: May 16, 2016

DOI: 10.1021/acs.langmuir.6b00230
Langmuir 2016, 32, 5946−5954

These amphiphilic molecules, when complexed with the polymer, added significantly to the hydrophobicity of the complex and increased polyarginine's solubility in hydrophobic environments. This even occurred when the amphiphiles were lipids integrated into the vesicle bilayer. For example, an increase of anionic egg yolk phosphatidylglycerol (EYPG) content, and thus the negative charge of otherwise zwitterionic egg yolk phosphatidylcholine (EYPC) membranes, led to a dramatic increase in dye release activity.[23] Isothermal calorimetry studies of the binding energy associated with nonaarginine show that while the peptide has a strong association with anionic distearoylphosphatidylglycerol (DSPG) vesicles, there is no such association with zwitterionic distearoylphosphatidylcholine (DSPC) vesicles.[31] Similarly, plasmon waveguide resonance studies of the PTD penetration with EYPC and EYPG lipid bilayers showed a higher affinity of this PTD for the anionic EYPG membrane.[28] It was thus assumed that the anionic content was necessary for membrane activity.

However, the notion that the presence of anionic charges on lipid membranes is the most important parameter for PTD(M)−membrane interaction is not unchallenged. In one study, a detailed kinetic analysis of the PTD tp10, a lysine-rich helical peptide, with vesicle systems featuring different anionic lipid content, was reported. This data revealed that while tp10 had stronger binding to more anionic vesicles, the actual rate of dye efflux from the different vesicles was not measurably altered.[32] This occurred because the rate of dye efflux depended strongly on the timespan the polymer stayed integrated into the bilayer, which was similar for both anionic and zwitterionic systems. Perhaps the most relevant study in this context is the investigation by Hennig et al.[25] with a polymer very similar to PTDM-**1** described below. With this polymer, dye release was measured against a series of vesicles with progressively increasing amounts of anionic EYPG. Unlike the study with the lysine-rich tp10, dye release dramatically *decreased* with increasing anionic content when using that guanidine-rich PTDM. This is strong supporting evidence that this class of guanidinium-rich ROMP polymers interacts in a fundamentally different way with lipid bilayers than arginine-rich peptides and that their interactions with lipid bilayers deserves separate analysis.[33] We therefore suggest the working hypothesis that there are two separate classes of PTDs and PTDMs: those, like polyarginine, which have an increased uptake in the presence of anionic lipids, and those, like tp10 and ROMP PTDMs, which have decreased activity. It is not understood why this latter class of compounds is different than the first, and in this study, we used a combination of polymer design and biophysical experiments to explore these questions.

MATERIALS AND METHODS

Materials. Maleic anhydride, maleimide, furan, 4-(dimethylamino)-pyridine (DMAP), 1-(3-(dimethylamino)propyl)-3-ethylcarbodiimide hydrochloride (EDC), methanol, 1,3-di-Boc-2-(2-hydroxyethyl)-guanidine, benzyl alcohol, ethyl vinyl ether, and trifluoroacetic acid (TFA) were obtained as reagent grade from Aldrich, Fluka, or Acros and used as received. Third generation Grubbs catalyst (dichloro-di(3-bromopyridino)-*N*,*N*′-dimesitylenoimidazolino-Ru = CHPh; G3) was synthesized as described previously by Grubbs et al.[34] The HPLC grade solvents, ethyl acetate, pentane, and hexane, were purchased from Aldrich, Fisher Scientific, or Acros and used as received. Tetrahydrofuran (THF) (HPLC grade, Fisher Scientific) was distilled from sodium/benzophenone under nitrogen. Dichloromethane (DCM) (HPLC grade, Fisher Scientific) was distilled from CaH_2 under nitrogen. Polycarbonate membranes (0.2 and 0.05 μm), egg yolk phosphatidylcholine (EYPC), porcine brain phosphatidylserine, (Brain PS), dioleoylphosphatidylcholine (DOPC), and dioleoyl-phosphatidylserine (DOPS) were purchased from Avanti Polar Lipids Inc. 5(6)-Carboxyfluorescein (CF) was purchased from Fluka. HEPES, sodium chloride, and 1 M NaOH solution were obtained from Sigma-Aldrich (Germany). Filters with a hydrophobic PTFE membrane and 0.2 μm pore size were obtained from Millipore.

PTDM Synthesis. Monomer synthesis was similar to that performed in previous reports.[26,27,35] The monomers are shown in Supporting Information Figure S1. PTDMs were synthesized by ring-opening metathesis polymerization with Grubbs third generation catalyst using previously reported methods.[27,35−37] Details of the synthesis, along with NMR and GPC characterization, are presented in the Supporting Information.

Dye Release Experiments. Dye release experiments were used to quantify the interaction of PTDMs with model membranes. Details of the dye-loaded vesicle preparation are presented in the Supporting Information. Dye release experiments were done similarly to previously published procedures.[35] In short, vesicles were loaded with the self-quenching fluorescent dye carboxyfluorescein and purified. A defined concentration of PTDM was then added to a defined amount of vesicles, and the dye efflux was quantified by measuring the fluorescence of the system. This was repeated for various PTDM concentrations, so that a curve of dye efflux versus polymer concentration was obtained. By fitting this curve as described below, the concentration that causes 50% of the maximal dye release of the system, EC_{50}, was determined. In our particular case, the experiment was performed as follows: 1960 μL of Tris buffer (10 mM Tris, 107 mM NaCl, pH 7.5) was added to the wells of a 12-well plate. 20 μL of 250 μM vesicle solution (as defined above) was added to each well, creating an in-well concentration of 2.5 μM. A plate reader to quantify fluorescence was heated to 25 °C before continuing. The plates were shaken at 25 °C and after 3 min a baseline fluorescence measurement, F_0, was taken. 20 μL of polymer/DMSO solutions containing varying concentrations (0.01−1000 μL) of polymer was added into wells with stirrers, and the plate was returned to the reader for 10 min of shaking. After 10 min, another reading, F_{10}, was taken. 20 μL of 5% Triton X-100 in DMSO was added to the wells, and after 3 min a final measurement, F_T, was taken. F_T and F_0 allowed use to normalize fluorescence to measure the fractional dye release:

$$Y = (F_{10} - F_0)/(F_T - F_0) \quad (1)$$

The fractional dye release Y was then fitted as a function of concentration, c, to the Hill equation by a least-squares method:

$$Y = Y_m \frac{(c/EC_{50})^n}{1 + (c/EC_{50})^n} \quad (2)$$

where EC_{50} is the concentration of 50% of maximal dye release and n is a fitting parameter.

Particle Mean Size and Zeta Potential Measurement. Vesicle preparation for this experiment is described in the Supporting Information. As with the dye release experiments above, varying concentrations of polymer were added to a vesicle solution containing 2.5 μM lipid under constant agitation. After 10 min, the solution was injected into a Malvern DTS 1061 folded capillary cell; dynamic light scattering measurements were immediately recorded, and the number-average mean size of the particles in solution was determined. Zeta potential was then measured on the same sample.

Surface Plasmon Resonance Spectroscopy. A lipid vesicle preparation and SPR working conditions are detailed in the Supporting Information. Polymer (4×10^{-4} mmol) was dissolved in 100 μL of DMSO and diluted with HEPES buffer to a concentration of 10 μM. Prior to use, all solutions were freshly prepared and filtered (0.20 μm). The SPR sensor was mounted into the SPR flow cell which was connected to the peristaltic pump. The lipid film on the SPR sensor was produced by flowing the vesicle solution over the chip (3 μL/min) until a plateau was reached (at least 3600 s contact time,

DOI: 10.1021/acs.langmuir.6b00230
Langmuir 2016, 32, 5946−5954

which corresponds to 18× the flow cell volume). A short injection of 10 mM NaOH (30 μL/min, 240 s, 12× flow cell volume) was used to remove loose vesicles, followed by rinsing with HEPES buffer (30 μL/min, 240 s and 5 μL/min, 300 s) to obtain a constant signal. The surface was then kept under buffer until polymer injection. For each measurement, a fresh lipid sensor was used. First, HEPES buffer was pumped over the lipid surface until a constant signal was obtained (5 μL/min, 600 s). Next, the polymer solution (5 μL/min, 1200 s, 10× flow cell volume) was injected, yielding the adsorption curves. Finally, HEPES buffer was injected until a constant signal was reached (5 μL/min, at least 3600 s) to obtain the desorption curves. The amount of bound polymer was measured in RU under the same conditions as with the lipid measurements. To make sure that the DMSO concentration did not cause changes in the lipid film, DMSO in buffer at the same concentrations as in the polymer solutions was injected. The effect on the SPR signal was found to be negligible.

RESULTS AND DISCUSSION

We synthesized three guanidine-rich PTDM polymers with tailor-made properties. The polymers (Figure 1) are statistical

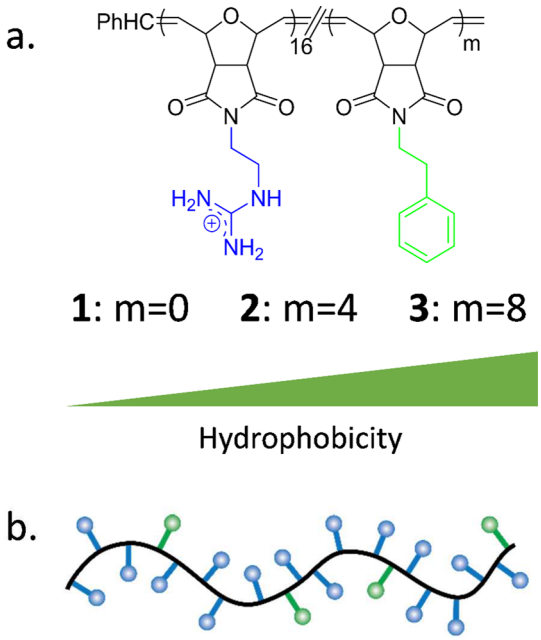

Figure 1. Polymer design used for this study. (a) Generic structure for the PTDM series. The different amounts of hydrophobic repeat units through the series, by variation of *m*, cause a hydrophobicity gradient at constant charge density. (b) Cartoon representation of random copolymer with 16 charged groups and 4 hydrophobic groups.

copolymers with a positively charged guanidinium residue and a hydrophobic phenyl residue on their respective repeat units and were obtained by ring-opening metathesis polymerization (ROMP). They have an average of 16 charges per polymer chain and additionally *m* hydrophobic repeat units (*m* = 0, 4, and 8 for PTDM **1**, **2**, and **3**, respectively). This corresponds to a hydrophobic fraction of 0%, 20%, and 33%. Thus, these three polymers had gradually increasing hydrophobicity. (Higher hydrophobic content was not investigated because we expected that the solubility of such hydrophobic polymers in aqueous media would be lower, which would lead to aggregation and thus bias our experiments.) Additionally, assuming that the distance between each polymer repeat unit is larger than or equal to the Bjerrum length in aqueous solution, this molecular design of the three polymers assured that they have the same molecular charge density. Therefore, they are expected to have similar electrostatic interactions with anionic surfaces, while the hydrophobicity gradient through the series affects their water and lipid solubility.

We exposed these three PTDMs to two types of phospholipid membranes with different anion lipid content: zwitterionic ones made from pure phosphatidylcholine (either natural egg yolk phosphatidylcholine (EYPC) or synthetic 1,2-dioleoyl-*sn*-glycero-3-phosphocholine (DOPC)) and partially anionic ones made from a 80:20 wt % mixture of phosphatidylcholine (EYPC or DOPC) and natural L-α-phosphatidylserine (Brain PS).

Three sets of experiments were performed with this system: First, the effect of anionic lipid content on membrane permeabilization was investigated with dye release studies. Second, the effect of surface charge differences on the size and zeta potential of the polymer–vesicle aggregates was examined. Third, the relative effects of vesicle anionic lipid content and polymer hydrophobicity on the membrane association of the polymer were quantified using surface plasmon resonance spectroscopy (SPR).

Dye Release Studies. We produced phospholipid vesicles loaded with a self-quenching fluorescent dye from the two membrane types under investigation. When these were exposed to the PTDMs at different polymer concentrations, their membrane was gradually permeated and their dye cargo was released. This resulted in a measurable increase in fluorescence of the polymer–vesicle solution (Figure 2). In most cases, a typical sigmoidal dye release curve was obtained. The turning point of this curve, called EC_{50}, corresponds to the concentration at 50% of the maximum fluorescence of the given vesicle–PTDM system and is a measure for the amount of PTDM needed to generate ∼50% dye release. The fluorescence plateau in the high concentration range corresponds to the maximum leakage of the given system. As shown in Table 1 and Figure 2, the EC_{50} for all three PTDMs, when in contact with the zwitterionic vesicles (0.0073–0.014 μM), differs only by a small factor and does not scale linearly with hydrophobicity. Within the accuracy of the experiment, those values can be considered similar. However, the maximum fluorescence is significantly higher for the two more hydrophobic polymers, demonstrating that the total dye released increases for the two hydrophobic PTDMs. The EC_{50} for the anionic vesicles (0.067–0.085 μM) is significantly higher than for the zwitterionic ones, by almost 1 order of magnitude. For the PTDM **1**–anionic vesicle combination, the curve does not have the sigmoidal curve shape necessary to define an EC_{50}. Yet, from analogy to the other five polymer–vesicle systems, it can be assumed that the curve is just featureless because the dye leakage is overall low and that the EC_{50} for PTDM **1** should be in the same range as for PTDMs **2** and **3**. (This assumption is supported by the surface plasmon resonance data discussed later.) As in the case of the zwitterionic vesicles, more hydrophobicity on the PTDMs also led to significantly higher dye release for the anionic vesicles. For PTDMs **2** and **3**, the primary difference between the dye release curves of the anionic and the zwitterionic vesicle systems is the amount of PTDM needed for dye release. It is worth noting here that we are only looking at dye release, not membrane activity which is a more complex series of interactions. For example, one important aspect of membrane activity is the ability of a polymer to bind at the solution–membrane interface, and it may well do so without damaging the membrane or causing dye

DOI: 10.1021/acs.langmuir.6b00230
Langmuir 2016, 32, 5946–5954

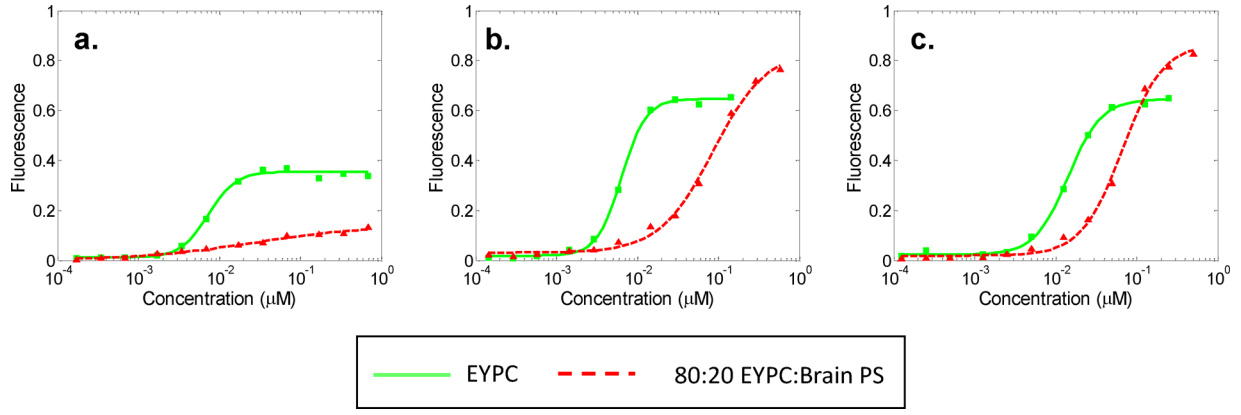

Figure 2. Dye release for (a) PTDM **1**, (b) PTDM **2**, and (c) PTDM **3** from carboxyfluorescein-loaded EYPC vesicles (green squares) and 80:20 EYPC:Brain PS vesicles (red triangles). Green lines and red dashes are fits to the data using the Hill equation, a standard fit for dye-leakage curves.[23,25,38]

Table 1. EC_{50} Values for the Dye Release Experiments

	EYPC		80:20 EYPC:Brain PS			DOPC		80:20 DOPC:DOPS		
polymer	EC_{50} (μM)	F_{max}	EC_{50} (μM)	F_{max}	EC_{50} ratio	EC_{50} (μM)	F_{max}	EC_{50} (μM)	F_{max}	EC_{50} ratio
1	0.0073	0.35	N/A	N/A	>900					
2	0.0064	0.65	0.085	0.80	13	0.016	0.64	0.12	0.75	7.1
3	0.014	0.64	0.067	0.87	4.7					

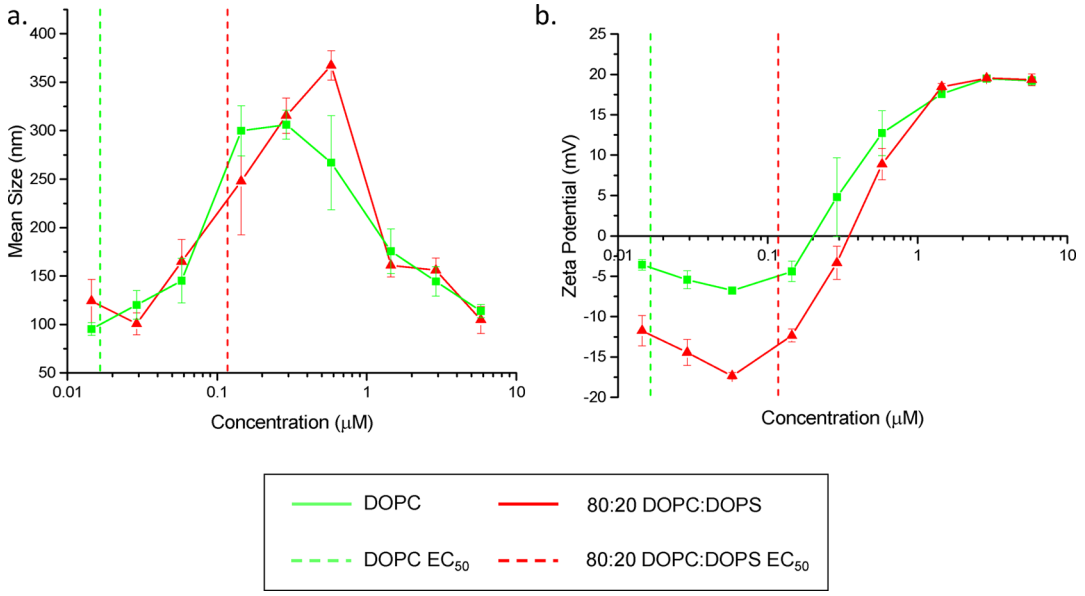

Figure 3. (a) Number mean particle size determined by dynamic light scattering and (b) zeta potential measurements for the interaction of varying concentrations of PTDM **2** with phospholipid vesicles. Green squares represent data for zwitterionic DOPC vesicles, while red triangles represent data for anionic 80:20 DOPC:DOPS vesicles. Green and red dashes represent the dye release EC50 values for the DOPC and 80:20 DOPC:DOPS vesicle systems, respectively.

to be released. (The surface plasmon resonance spectroscopy data shown later is evidence that this is the case for PTDM **1**.)

Size and Zeta Potential. The dye release data generally probes membrane permeability, but it cannot differentiate the various possible mechanisms by which dye is released, which range from transient pore formation or transduction to catastrophic vesicle rupture. We therefore studied the interaction of PTDM **2** with the same two vesicle types but this time using simultaneous zeta potential and vesicle size measurements. In this experiment, PTDM **2** was added at different concentrations to the anionic and zwitterionic vesicles, respectively, spanning the same phospholipid and polymer concentrations used in the dye leakage studies. The results are shown in Figure 3.

The size of the system was determined by dynamic light scattering at a single angle. This is not optimal for such nonisocratic scatterers, and the size data therefore has to be treated with care. However, we were less interested in the absolute size data than understanding whether the light scattering signal increases, which would mean aggregation, or goes to zero, which would mean that the vesicles are ruptured as the PTDM is added. As the zeta potential of the PTDM–

DOI: 10.1021/acs.langmuir.6b00230
Langmuir 2016, 32, 5946−5954

vesicle system was measured simultaneously, the correlation of the two parameters yielded valuable information about the system under investigation.

As can be seen from Figure 3a, the vesicles had an initial diameter of 100 nm, as expected given their preparation method. When PTDM **2** was titrated into the vesicles, there was a factor of 3−4 increase in size, most likely due to aggregated vesicles. The size curve goes through a peak at a concentration of about 0.2 μM for the zwitterionic vesicles and about 0.6 μM for the anionic vesicles. It then gradually goes back to the original 100 nm at around 6 μM polymer concentration. Remarkably, it does not go below that value, suggesting that the vesicles survive this process intact. Another interesting feature of the size curve is that it is very similar for both types of vesicles: initial slope, position and height of the peak maximum, and the leveling off at higher polymer concentrations seem to indicate that these two vesicle types behave the same when exposed to PTDM **2**. The initial size increase can be explained by continuous aggregation. The cationic polymer binds to the vesicles, creating local positively charged patches, thus making them "sticky" despite their overall negative charge (see for example the dashed red line in Figure 3). This attractive electrostatic force is long-range; therefore, the vesicles start to aggregate when they diffuse within reach of each other. Eventually, the surface of the vesicles becomes saturated with adsorbed polymer and significantly cationic. At this point, the vesicles within the aggregates again become repellant for one another, and the aggregate disassembles. The peak of the anionic vesicles is slightly shifted to higher polymer concentration because more cationic polymer is needed before this saturation state is reached.

A comparison with the zeta potential curves yields even further insight into this process. Initially, the zeta potential of the zwitterionic polymers is slightly negative (−3 mV, presumably due to anion adsorption from solution), while the anionic vesicles, expectedly, are more strongly negative (−12 mV). At lower concentrations, the added PTDM **2** does not significantly change these values. Then, however, the isoelectric point is reached (0.2 μM for the zwitterionic vesicles and 0.4 μM for the anionic vesicles), and the zeta potential curve becomes sigmoidal, with a plateau at about 18 mV. When comparing this data with the simultaneously measured size curve, it is interesting to note that the PTDM concentration at the isoelectric point corresponds to the PTDM concentration of the size peak for each vesicle type. This corroborates the above interpretation of the polymer−vesicle interaction: at the isoelectric point, all charges are compensated, and there is no electrostatic driving force for the aggregate to further grow. Once more cationic charge is added (positive zeta potential), the vesicles become repellant and the aggregate falls apart. The plateau in the zeta potential then corresponds to a fullly PTDM-covered vesicle. The PTDM cannot further adsorb at the vesicle surface because there is no more enthalpic gain for doing so. This has to happen at the same zeta potential for both vesicle types because it is the electrostatic repulsion of the charged vesicle with incoming polymer chains that determines the saturation point, not the initial charge of the vesicles. This result is consistent with studies of the interaction of cationic polymers with anionic particles, which show maximum particle aggregation at charge neutralization, with reduced aggregate sizes at both lower and higher polymer concentrations.[39−41]

For further interpretation of the dye release data, the combined light scattering data−zeta potential data tells us one important feature. While the dye release studies do not distinguish between dye released by membrane permeabilization and dye released by vesicle disruption, the light scattering data suggests that these vesicles remain largely intact at concentrations relevant to dye release. This suggests that the dye release functions by some process other than simple membrane disintegration.

Surface Plasmon Resonance Spectroscopy. To further examine the interaction of our PTDM series and the test vesicles, we turned to surface plasmon resonance spectroscopy (SPR). SPR relies on the plasmon resonance phenomenon, where for a specific incidence angle p-polarized light cast onto a gold-plated sensor is absorbed by the gold layer and turned into a surface wave (plasmon).[42−45] The detection angle of the plasmon minimum shifts as matter adsorbs on the gold layer because this alters the dielectric properties of the surface. Thus, by monitoring the reflectivity signal intensity at a single angle on the leading slope of the plasmon, it is possible measure the real-time surface adsorption of an analyte.

While the dye release and zeta potential experiments had identical lipid and PTDM concentrations, the SPR experiments had to be performed differently. The setup is such that a lipid bilayer was formed on the gold sensor (see Supporting Information for details), and a polymer solution of fixed concentration was continuously flowed over that bilayer. Thus, the only limit on the amount of PTDM interaction with the lipid bilayer is the kinetics of the PTDM−bilayer interaction and the maximum adsorbance capacity of the lipid layer. The results of the SPR kinetics experiments are shown in Figure 4 for each PTDM−vesicle combination. First, a baseline of buffer flowing over the bilayer was recorded. At t = 0, PTDM at a concentration of 10 μM was injected, and the adsorption curve was recorded until t = 20 min. The system was then switched back to a continuous flow of buffer, and the polymer desorption was monitored until t = 60 min. As can be seen from the data, the curves for all three PTDMs have a higher maximum for the anionic vesicles.

Assuming similar refractive indices for all three PTDMs, there is another clear trend: for both vesicle types, the more hydrophobic the PTDM, the more PTDM adsorbed. While some loosely bound material is removed by the washing step at 20 min, the vast majority of PTDM stays adsorbed to the surface.

The SPR data (Figure 4 and Table 2) corroborates the dye leakage data. The relative differences between the amount of adsorbed polymer on the zwitterionic vesicles and the anionic ones, after buffer, are 1.2 RU for PTDM **1**, 1.9 RU for PTDM **2**, and 6.1 RU for PTDM **3**. Within the PTDM series, the differences in adsorption after washing between PTDM **1** and **3** are 10.8 RU for the zwitterionic vesicles and 15.7 RU for the anionic vesicles. Thus, in each case, the PTDM adsorbs more strongly to the anionic lipid system than to the purely zwitterionic one; however, this effect is dwarfed by the increase in adsorption due to the differences in polymer hydrophobicity. Not all of the PTDM dissociates from the membrane during this process, which would indicate that some of the PTDM remains either embedded in the membrane or inextricably bound to it. It is also worth noting that the relative amount of polymer removed from the membrane after a prolonged buffer flow was relatively independent of both membrane composition and polymer hydrophobicity (1.9−3.4 RU, see Table 2). This indicates that the amount of PTDM that remains removable on the surface is the same for all experiments. Differences in

DOI: 10.1021/acs.langmuir.6b00230
Langmuir 2016, 32, 5946−5954

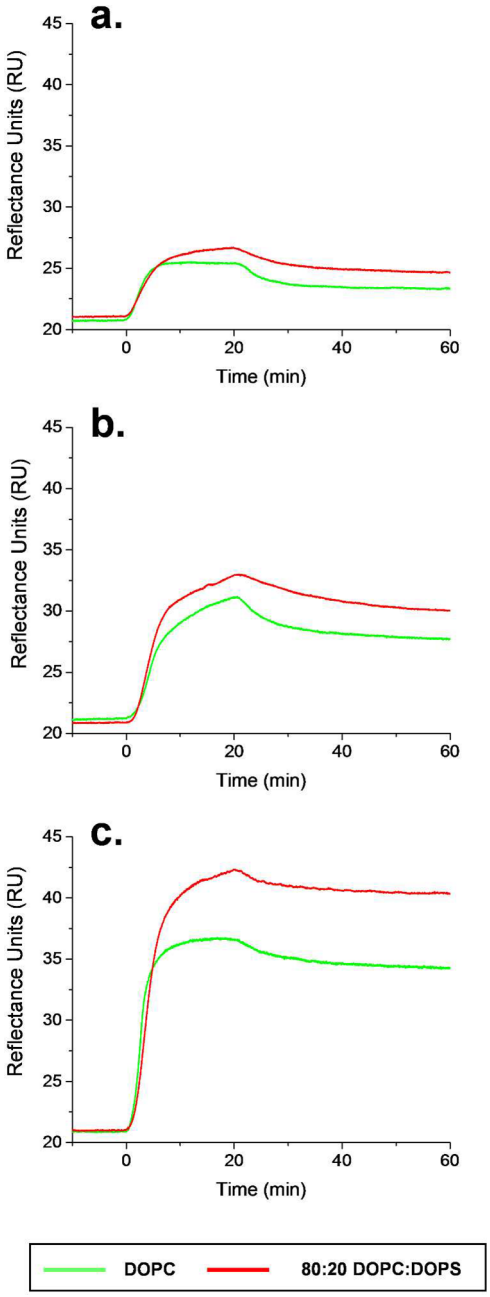

Figure 4. Surface plasmon resonance spectroscopy adsorption and desorption curves for 10 μM of PTDMs: (a) **PTDM 1**, (b) **PTDM 2**, (c) **PTDM 3**. Reflectivity signal intensity (in arbitrary units) is plotted versus time. Green lines represent adsorption to the zwitterionic DOPC lipid system, while red lines represent adsorption to the anionic DOPC:DOPS system. The bilayer was exposed to a continuous flow of polymer solution starting at t = 0 and then flushed with buffer starting at t = 20 min.

Table 2. Peak and Final Change in Reflectance for SPR Experiments

	DOPC		DOPC:DOPS	
PTDM	peak (RU)	after buffer (RU)	peak (RU)	after buffer (RU)
1	4.7	2.5	5.7	3.7
2	10.6	7.2	12.1	9.1
3	15.8	13.3	21.3	19.4

adsorption magnitude, then, are due to polymer that associates with the membrane in a permanent manner and due to the nature of that membrane.

To sum up the results of all three methods: dye release studies, size/zeta potential studies, and SPR experiments unanimously demonstrated that the anionic vesicles can take up more PTDM than the zwitterionic ones in all three cases. Size/zeta potential studies further show that dye release does not correlate with vesicle size reduction and that the dye is therefore released by an increased membrane permeabilization and not by vesicle rupture. Dye release studies further show that the highly hydrophilic PTDM **1** hardly causes any membrane permeabilization, although according to SPR, a substantial amount is adsorbed (about 1/3 of the amount of PTDM **3**, assuming the SPR data scales linearly). The two more hydrophobic PTDMs cause significantly more dye release, and at the same time much more of them is adsorbed on the bilayer, as evidenced by the SPR data. Also, this binding is much less reversible. When comparing the relative effects of more charge on the vesicles (which enhances the electrostatic interaction) with more hydrophobicity on the PTDM (which strengthens the ability of the polymer to permeate membranes), it also seems clear from the dye leakage studies that the added negative charge on the vesicles only dictates that more overall polymer is needed to cause leakage, but the membrane charge had very little effect on the maximal amount of leakage, which seemed to be dictated by the polymer hydrophobicity.

The remaining question is what this interpretation means for the series of events with the lipid membrane and for the way we consider PTDM–membrane interactions. The "adaptive translocation" model that is frequently proposed for PTDs and PTDMs states that the anionic lipid assists the polymer transport across the membrane.[24] The dye leakage data states that we need significantly more polymer to obtain dye leakage for vesicles with anionic lipid content compared to purely zwitterionic ones. That means that a portion of the cationic polymer appears to be "consumed" by the anionic lipid and likely "pinned" to the membrane. We also see, however, that the PTDMs that cause significant dye leakage do so *more* efficiently in the presence of anionic lipid (cf. PTDM **2** and **3** on the anionic vesicles). The pinning of the PTDM on the membrane certainly changes the local fluidity of the membrane; it also likely changes the local concentration. The result is increased permeability, and in this respect, the anionic lipids can be considered to assist membrane permeabilization. In other words, while some of the PTDMs are pinned at the membrane until charge neutralization has been obtained (cf. zeta potential data), once this point is reached, the next PTDMs may find it easier to then traverse the membrane.

However, it is also clearly visible that the role of hydrophobicity for membrane translocation has been largely underestimated. Both the dye leakage data and the SPR data beautifully illustrate that charge is not everything. While there was the same number of charges on all three PTDM, the hydrophilic PTDM **1** shows little dye release and a lower amount of membrane association. We interpret this as surface coverage of the vesicle with PTDM **1**, but very little actual membrane insertion. Since the number of sites on the surface is limited, membrane association of PTDM **1** stops once the vesicle is covered. PTDMs **2** and **3**, on the other hand, can insert into the membrane more significantly due to their hydrophobic content. When looking carefully at the SPR curves

DOI: 10.1021/acs.langmuir.6b00230
Langmuir 2016, 32, 5946–5954

of PTDM **2**, it seems like there are two regimes: one initial adsorption step, then a deviation from the expected exponential, as if the adsorption of PTDM 2 consists of a two-step process: first, association at the membrane through electrostatics and, then, insertion into the membrane through hydrophobic interaction. For PTDM **2**, these two regimes are more clearly visible in the SPR curve than for PTDM **3**. This could be explained by the membrane insertion being slower than the electrostatic association: only when the insertion takes place, sites become available at the surface, so that the first step of the binding is controlled by the kinetics of the insertion step. For PTDM **3**, the most hydrophobic polymer, insertion is faster, so that the second regime is not so pronounced in the SPR curves of PTDM **3** and the overall membrane association kinetics are more closely exponential than for PTDM **2**.

CONCLUSIONS

We investigated the interaction of novel ROMP-based PTDM polymers with constant charge density but gradually increasing hydrophobicity with both anionic and zwitterionic lipid membranes. These systems were studied using a combination of dye-leakage assays, simultaneous measurements of zeta potential and aggregate sizes, and surface plasmon resonance spectroscopy.

The dye release data demonstrates conclusively that the introduction of anionic lipid to phospholipid membranes presents a barrier to PTDM activity because it pins some of the cationic PTDMs to the surface, thus requiring an overall higher PTDM concentration to obtain dye leakage. However, this barrier can be overcome with the addition of hydrophobic moieties to the polymer, and in fact once membrane permeabilization is obtained, the extent of permeabilization is higher for vesicles with anionic content than for purely zwitterionic ones. Light scattering data and zeta potential measurements showed that PTDM **2** had similar surface-association behavior with both anionic and zwitterionic lipid systems and that this binding does not induce membrane rupture. SPR data indicates that the increase in binding due to the presence of anionic lipid is far smaller than that due to added polymer hydrophobicity.

From this data, then, a clearer picture of how these polymers are able to translocate phospholipid membranes begins to appear. The first step is a membrane association driven by electrostatic interaction. Once on the lipid surface, anionic content on the surface "pins" the cationic polymer on the outer leaflet of the lipid bilayer and likely prevents further penetration, unless more PTDM is added. However, as polymer hydrophobicity is increased, there is a significant driving force for the PTDM to partition into the hydrophobic domain of the lipid bilayer, overcoming that electrostatic pinning and at the same time making space for further PTDM molecules to surface-associate.

It is important to remark that the implications of this study may be limited to this particular PTDM design (or those PTDMs based on hydrocarbon backbones). As mentioned in the Introduction, similar studies of the effect of anionic lipid on the activity of oligo- and polyarginine have produced very different results. While the exact reason for this discrepancy is still unclear, it is likely that the ROMP-based PTDM activity is influenced by the hydrophobicity of the PTDM backbone, in addition to the side chain hydrophobicity. Peptide-based PTDs such as polyarginine are substantially less hydrophobic. Thus, while the relative difference in membrane association of ROMP PTDMs **2** and **3** on anionic and zwitterionic lipid systems, respectively, is small compared to the hydrophobicity effect, that relative difference may be much larger for polyarginine. It was previously observed that the arginine oligomer R9 alone does not induce dye release in EYPC vesicles except in very high concentrations,[23] so it is perhaps no surprise that this polymer system produces mechanistically different results.

To conclude, the results for our more hydrophobic PTDMs are important because they provide guidelines for the design of new and superior polymers for cellular uptake as well as insight into the physics of this apparently unique membrane transporting molecules.

ASSOCIATED CONTENT

Supporting Information

The Supporting Information is available free of charge on the ACS Publications website at DOI: 10.1021/acs.langmuir.6b00230.

Additional synthetic methods and dye release data (PDF)

AUTHOR INFORMATION

Corresponding Authors

*E-mail tew@mail.pse.umass.edu (G.N.T.).
*E-mail lienkamp@imtek.uni-freiburg.de (K.L.).

Funding

This work was funded by the NSF (DMR-1308123). Funding by the Emmy-Noether program of the Deutsche Forschungsgemeinschaft (German research foundation, DFG; LI1714/5-1) and the Klaus-Murmann-Stiftung (sdw) is gratefully acknowledged.

Notes

The authors declare no competing financial interest.

REFERENCES

(1) Frankel, A. D.; Pabo, C. O. Cellular uptake of the tat protein from human immunodeficiency virus. *Cell* **1988**, *55* (6), 1189−1193.

(2) Green, M.; Loewenstein, P. M. Autonomous functional domains of chemically synthesized human immunodeficiency virus tat trans-activator protein. *Cell* **1988**, *55* (6), 1179−1188.

(3) Fawell, S.; Seery, J.; Daikh, Y.; Moore, C.; Chen, L. L.; Pepinsky, B.; Barsoum, J. Tat-mediated delivery of heterologous proteins into cells. *Proc. Natl. Acad. Sci. U. S. A.* **1994**, *91* (2), 664−668.

(4) Deshayes, S.; Morris, M.; Heitz, F.; Divita, G. Delivery of proteins and nucleic acids using a non-covalent peptide-based strategy. *Adv. Drug Delivery Rev.* **2008**, *60* (4−5), 537−547.

(5) Heitz, F.; Morris, M. C.; Divita, G. Twenty years of cell-penetrating peptides: from molecular mechanisms to therapeutics. *Br. J. Pharmacol.* **2009**, *157* (2), 195−206.

(6) Snyder, E. L.; Dowdy, S. F. Cell Penetrating Peptides in Drug Delivery. *Pharm. Res.* **2004**, *21* (3), 389−393.

(7) Mäe, M.; Langel, Ü. Cell-penetrating peptides as vectors for peptide, protein and oligonucleotide delivery. *Curr. Opin. Pharmacol.* **2006**, *6* (5), 509−514.

(8) Kim, H. Y.; Yum, S.; Jang, G. Y.; Ahn, D.-R. Discovery of a non-cationic cell penetrating peptide derived from membrane-interacting human proteins and its potential as a protein delivery carrier. *Sci. Rep.* **2015**, *5*, 11719.

(9) Marie, E.; Sagan, S.; Cribier, S.; Tribet, C. Amphiphilic Macromolecules on Cell Membranes: From Protective Layers to Controlled Permeabilization. *J. Membr. Biol.* **2014**, *247* (9−10), 861−881.

(10) Wender, P. A.; Galliher, W. C.; Goun, E. A.; Jones, L. R.; Pillow, T. H. The design of guanidinium-rich transporters and their

DOI: 10.1021/acs.langmuir.6b00230
Langmuir 2016, 32, 5946−5954

internalization mechanisms. *Adv. Drug Delivery Rev.* **2008**, *60* (4−5), 452−472.
(11) Richard, J. P.; Melikov, K.; Vives, E.; Ramos, C.; Verbeure, B.; Gait, M. J.; Chernomordik, L. V.; Lebleu, B. Cell-penetrating Peptides. *J. Biol. Chem.* **2002**, *278* (1), 585−590.
(12) Nakase, I.; Niwa, M.; Takeuchi, T.; Sonomura, K.; Kawabata, N.; Koike, Y.; Takehashi, M.; Tanaka, S.; Ueda, K.; Simpson, J. C.; Jones, A. T.; Sugiura, Y.; Futaki, S. Cellular Uptake of Arginine-Rich Peptides: Roles for Macropinocytosis and Actin Rearrangement. *Mol. Ther.* **2004**, *10* (6), 1011−1022.
(13) Takeuchi, T.; Kosuge, M.; Tadokoro, A.; Sugiura, Y.; Nishi, M.; Kawata, M.; Sakai, N.; Matile, S.; Futaki, S. Direct and Rapid Cytosolic Delivery Using Cell-Penetrating Peptides Mediated by Pyrenebutyrate. *ACS Chem. Biol.* **2006**, *1* (5), 299−303.
(14) Al-Taei, S.; Penning, N. A.; Simpson, J. C.; Futaki, S.; Takeuchi, T.; Nakase, I.; Jones, A. T. Intracellular Traffic and Fate of Protein Transduction Domains HIV-1 TAT Peptide and Octaarginine. Implications for Their Utilization as Drug Delivery Vectors. *Bioconjugate Chem.* **2006**, *17* (1), 90−100.
(15) Futaki, S. Membrane-permeable arginine-rich peptides and the translocation mechanisms. *Adv. Drug Delivery Rev.* **2005**, *57* (4), 547−558.
(16) Gump, J. M.; Dowdy, S. F. TAT transduction: the molecular mechanism and therapeutic prospects. *Trends Mol. Med.* **2007**, *13* (10), 443−448.
(17) Tezgel, A. Ö.; Gonzalez-Perez, G.; Telfer, J. C.; Osborne, B. A.; Minter, L. M.; Tew, G. N. Novel Protein Transduction Domain Mimics as Nonviral Delivery Vectors for siRNA Targeting NOTCH1 in Primary Human T cells. *Mol. Ther.* **2013**, *21* (1), 201−209.
(18) Tezgel, A. O. Protein Transduction Domain Mimics by ROMP and Their Bioactive Cargo Delivery. PhD, University of Massachusetts Amherst, February 2013.
(19) Gait, M. J. Peptide-mediated cellular delivery of antisense oligonucleotides and their analogues. *Cell. Mol. Life Sci.* **2003**, *60* (5), 844−853.
(20) Moulton, H. M.; Moulton, J. D. Arginine-rich cell-penetrating peptides with uncharged antisense oligomers. *Drug Discovery Today* **2004**, *9* (20), 870.
(21) Nagahara, H.; Vocero-Akbani, A. M.; Snyder, E. L.; Ho, A.; Latham, D. G.; Lissy, N. A.; Becker-Hapak, M.; Ezhevsky, S. A.; Dowdy, S. F. Transduction of full-length TAT fusion proteins into mammalian cells: TAT-p27Kip1 induces cell migration. *Nat. Med.* **1998**, *4* (12), 1449−1452.
(22) Zatsepin, T.; Turner, J.; Oretskaya, T.; Gait, M. Conjugates of Oligonucleotides and Analogues with Cell Penetrating Peptides as Gene Silencing Agents. *Curr. Pharm. Des.* **2005**, *11* (28), 3639−3654.
(23) Sakai, N.; Matile, S. Anion-Mediated Transfer of Polyarginine across Liquid and Bilayer Membranes. *J. Am. Chem. Soc.* **2003**, *125* (47), 14348−14356.
(24) Nishihara, M.; Perret, F.; Takeuchi, T.; Futaki, S.; Lazar, A. N.; Coleman, A. W.; Sakai, N.; Matile, S. Arginine magic with new counterions up the sleeve. *Org. Biomol. Chem.* **2005**, *3* (9), 1659−1669.
(25) Hennig, A.; Gabriel, G. J.; Tew, G. N.; Matile, S. Stimuli-Responsive Polyguanidino-Oxanorbornene Membrane Transporters as Multicomponent Sensors in Complex Matrices. *J. Am. Chem. Soc.* **2008**, *130* (31), 10338−10344.
(26) Som, A.; Reuter, A.; Tew, G. N. Protein Transduction Domain Mimics: The Role of Aromatic Functionality. *Angew. Chem., Int. Ed.* **2012**, *51* (4), 980−983.
(27) Som, A.; Tezgel, A. O.; Gabriel, G. J.; Tew, G. N. Self-Activation in De Novo Designed Mimics of Cell-Penetrating Peptides. *Angew. Chem., Int. Ed.* **2011**, *50* (27), 6147−6150.
(28) Alves, I. D.; Bechara, C.; Walrant, A.; Zaltsman, Y.; Jiao, C.-Y.; Sagan, S. Relationships between Membrane Binding, Affinity and Cell Internalization Efficacy of a Cell-Penetrating Peptide: Penetratin as a Case Study. *PLoS One* **2011**, *6* (9), e24096.
(29) Alves, I. D.; Jiao, C.-Y.; Aubry, S.; Aussedat, B.; Burlina, F.; Chassaing, G. r.; Sagan, S. Cell biology meets biophysics to unveil the different mechanisms of penetratin internalization in cells. *Biochim. Biophys. Acta, Biomembr.* **2010**, *1798* (12), 2231−2239.
(30) Jiao, C.-Y.; Delaroche, D.; Burlina, F.; Alves, I. D.; Chassaing, G.; Sagan, S. Translocation and Endocytosis for Cell-penetrating Peptide Internalization. *J. Biol. Chem.* **2009**, *284* (49), 33957−33965.
(31) Walrant, A.; Correia, I.; Jiao, C.-Y.; Lequin, O.; Bent, E. H.; Goasdoué, N.; Lacombe, C.; Chassaing, G.; Sagan, S.; Alves, I. D. Different membrane behaviour and cellular uptake of three basic arginine-rich peptides. *Biochim. Biophys. Acta, Biomembr.* **2011**, *1808* (1), 382−393.
(32) Yandek, L. E.; Pokorny, A.; Florén, A.; Knoelke, K.; Langel, Ü.; Almeida, P. F. F. Mechanism of the Cell-Penetrating Peptide Transportan 10 Permeation of Lipid Bilayers. *Biophys. J.* **2007**, *92* (7), 2434−2444.
(33) Lein, M.; deRonde, B. M.; Sgolastra, F.; Tew, G. N.; Holden, M. A. Protein transport across membranes: Comparison between lysine and guanidinium-rich carriers (0006-3002 (print)).
(34) Love, J. A.; Morgan, J. P.; Trnka, T. M.; Grubbs, R. H. A practical and highly active ruthenium-based catalyst that effects the cross metathesis of acrylonitrile. *Angew. Chem., Int. Ed.* **2002**, *41* (21), 4035−7.
(35) Schmidt, N. W.; Lis, M.; Zhao, K.; Lai, G. H.; Alexandrova, A. N.; Tew, G. N.; Wong, G. C. L. Molecular Basis for Nanoscopic Membrane Curvature Generation from Quantum Mechanical Models and Synthetic Transporter Sequences. *J. Am. Chem. Soc.* **2012**, *134* (46), 19207−19216.
(36) Tezgel, A. O.; Telfer, J. C.; Tew, G. N. De Novo Designed Protein Transduction Domain Mimics from Simple Synthetic Polymers. *Biomacromolecules* **2011**, *12* (8), 3078−3083.
(37) Sgolastra, F.; Minter, L. M.; Osborne, B. A.; Tew, G. N. The Importance of Sequence Specific Hydrophobicity in Synthetic Protein Transduction Domain Mimics. *Biomacromolecules* **2014**, *15* (3), 812−820.
(38) Lienkamp, K.; Kumar, K.-N.; Som, A.; Nüsslein, K.; Tew; Gregory, N. "Doubly Selective" Antimicrobial Polymers: How Do They Differentiate between Bacteria? *Chem. - Eur. J.* **2009**, *15* (43), 11710−11714.
(39) Hierrezuelo, J.; Sadeghpour, A.; Szilagyi, I.; Vaccaro, A.; Borkovec, M. Electrostatic Stabilization of Charged Colloidal Particles with Adsorbed Polyelectrolytes of Opposite Charge. *Langmuir* **2010**, *26* (19), 15109−15111.
(40) Kleimann, J.; Gehin-Delval, C.; Auweter, H.; Borkovec, M. Super-Stoichiometric Charge Neutralization in Particle−Polyelectrolyte Systems. *Langmuir* **2005**, *21* (8), 3688−3698.
(41) Gabriel, G. J.; Pool, J. G.; Som, A.; Dabkowski, J. M.; Coughlin, E. B.; Muthukumar, M.; Tew, G. N. Interactions between Antimicrobial Polynorbornenes and Phospholipid Vesicles Monitored by Light Scattering and Microcalorimetry. *Langmuir* **2008**, *24* (21), 12489−12495.
(42) Knoll, W. INTERFACES AND THIN FILMS AS SEEN BY BOUND ELECTROMAGNETIC WAVES. *Annu. Rev. Phys. Chem.* **1998**, *49* (1), 569−638.
(43) Beseničar, M.; Maček, P.; Lakey, J. H.; Anderluh, G. Surface plasmon resonance in protein−membrane interactions. *Chem. Phys. Lipids* **2006**, *141* (1−2), 169−178.
(44) Morton, T. A.; Myszka, D. G.; Chaiken, I. M. Interpreting complex binding kinetics from optical biosensors: a comparison of analysis by linearization, the integrated rate equation, and numerical integration. *Anal. Biochem.* **1995**, *227* (1), 176−185.
(45) Mozsolits, H.; Aguilar, M.-I. Surface plasmon resonance spectroscopy: An emerging tool for the study of peptide−membrane interactions. *Biopolymers* **2002**, *66* (1), 3−18.
(46) Christensen, L. L. H. Theoretical Analysis of Protein Concentration Determination Using Biosensor Technology under Conditions of Partial Mass Transport Limitation. *Anal. Biochem.* **1997**, *249* (2), 153−164.
(47) Karlsson, R.; Roos, H.; Fägerstam, L.; Persson, B. Kinetic and Concentration Analysis Using BIA Technology. *Methods* **1994**, *6* (2), 99−110.

DOI: 10.1021/acs.langmuir.6b00230
Langmuir 2016, 32, 5946−5954

(48) Segel, L.; Slemrod, M. The Quasi-Steady-State Assumption: A Case Study in Perturbation. *SIAM Rev.* **1989**, *31* (3), 446−477.
(49) Myszka, D. G.; He, X.; Dembo, M.; Morton, T. A.; Goldstein, B. Extending the range of rate constants available from BIACORE: interpreting mass transport-influenced binding data. *Biophys. J.* **1998**, *75* (2), 583−594.

DOI: 10.1021/acs.langmuir.6b00230
Langmuir 2016, 32, 5946−5954